## 1 A novel framework for accurately quantifying wetland

## 2 depression water storage capacity with coarse-resolution

## 3 terrain data

- 4 Boting Hu<sup>1,2</sup>, Liwen Chen<sup>1</sup>, Yanfeng Wu<sup>1</sup>, Jingxuan Sun<sup>1,2</sup>, Y. Jun Xu<sup>3</sup>, Qingsong
- 5 Zhang<sup>1,2</sup>, Guangxin Zhang<sup>1</sup>
- 6 Northeast Institute of Geography and Agroecology, Chinese Academy of Sciences, Changchun, Jilin
- 7 130102, China
- 8 <sup>2</sup> University of Chinese Academy of Sciences, Beijing 100049, China
- 9 <sup>3</sup> School of Renewable Natural Resources, Louisiana State University Agricultural Center, 227
- 10 Highland Road, Baton Rouge, LA 70803, USA
- 11 Correspondence to: Guangxin Zhang (zhgx@iga.ac.cn)

12

13

14

15

16

17

18

19

20

21

22

23

24

25

26

27

28

29

Abstract. Accurate quantification of wetland depression water storage capacity (WDWSC) is imperative for comprehending the wetland hydrological regulation functions to support integrated water resources management. Considering the challenges posed by the high acquisition cost of high-resolution LiDAR DEM or the absence of field measurements for most wetland areas, urgent attention is required to develop an accurate estimation framework for WDWSC using open-source, low-cost, multi-source remote sensing data. In response, we developed a novel framework, WetlandSCB, utilizing coarse-resolution terrain data for accurate estimation of WDWSC. This framework overcame several technical difficulties, including biases in above-water topography, incompleteness and inaccuracy of wetland depression identification, and the absence of bathymetry. Validation and application of the framework were conducted in two national nature reserves of northeast China. The study demonstrated that integrating priority-flood algorithm, morphological operators and prior information can accurately delineate the wetland depression distribution with overall accuracy and Kappa coefficient both exceeding 0.95. The use of water occurrence map can effectively correct numerical biases in above-water topography with Pearson coefficient and R<sup>2</sup> increasing by 0.33 and 0.38 respectively. Coupling spatial prediction and modeling with remote sensing techniques yielded highly accurate bathymetry estimates, with <3% relative error compared to filed measurements. Overall, the WetlandSCB framework achieved estimation of WDWSC with <10%

relative error compared to field topographic and bathymetric measurements. The framework and its concept are transferable to other wetland areas globally where field measurements and/or high-resolution terrain data are unavailable, contributing to a major technical advancement in estimating WDWSC in river basins.

**Keywords**: Wetland depression; Water storage capacity; Hypsometric curve; coarse-resolution terrain data; wetland hydrological regulation functions

Wetlands are multifunctional ecosystems considered as nature-based solutions for effective water

36

37

38

39

40

41

42

43

44

45

46

47

48

49

50

51

52

53

54

55

56

57

58

59

30

31

32

33

34

35

#### 1 Introduction

management in river basins (Thorslund et al., 2017). They exert a profound influence on watershed hydrological processes and water resource availability through their hydrological regulation functions, such as maintaining baseflow, buffering floods, and delaying droughts (Acreman and Holden, 2013; Wu et al., 2023). These functions are essential for enhancing watershed resilience and ensuring water security (Cohen et al., 2016; Evenson et al., 2018; Lane et al., 2018). Wetland depression water storage capacity (hereafter abbreviated as WDWSC) represents a critical component of wetland hydrological regulation functions. The quantitative study of the WDWSC contributes to advancing scientific understanding of wetland hydrological regulation functions and to improving integrated water resources management at the watershed scale (Ahmad et al., 2020; Fang et al., 2019; Jones et al., 2018; Shook et al., 2021). The WDWSC can be defined as the maximum surface water volume that each wetland depression can store without spilling to down-gradient waters (Jones et al., 2018). Previous studies predominantly employed wetland depression identification algorithms to derive wetland depression topography from terrain data. In a vector-based contour representation, wetland depressions are shown as nested closed contours, with inner contours at lower elevations than the outer ones (Wu and Lane, 2016). Area-depth pairs are derived from the contour lines of wetland depressions, and hypsometric curves are constructed by applying curve-fitting methods to the obtained pairs (e.g., Haag et al., 2005; Wu and Lane, 2016). Therefore, the key determinants for the accuracy of the WDWSC calculation are the rationality of the wetland depression identification algorithms and the precision of terrain data. Many scholars have conducted research on wetland depression identification algorithms, which can be mainly categorized into three types: depression filling, depression breaching and hybrid combing both the filling and breaching approaches (Wu et al., 2019). Among these, the priority-flood algorithm within the depression filling category is widely adopted as a prevalent algorithm for wetland depression identification (Barnes et al., 2014; Lindsay, 2016; Wu et al., 2019; Zhou et al., 2016). The priority-flood algorithm works by flooding DEM cells inwards from their edges using a priority queue to determine the sequence of cells to be flooded. Wu et al. (2019) and Rajib et al. (2019) demonstrated the feasibility of accurately deriving wetland depression topography using the priority-flood algorithm in the Pipestem watershed and Upper Mississippi river basin, respectively. Bare-earth high-resolution airborne light detection and ranging (LiDAR) DEM can provide accurate topographic information of wetland depressions, significantly improving the estimation accuracy of the WDWSC. For example, Jones et al. (2018) used high-resolution LiDAR DEM to estimate WDWSC in the Delmarva Peninsula. However, the high acquisition cost of LiDAR DEM renders it impractical for large-scale estimation of WDWSC. The global open-access spaceborne-derived DEMs (hereafter referred as global DEMs), such as Shuttle Radar Topography Mission (SRTM), ALOS Global Digital Surface Model, the Terra Advanced Spaceborne Thermal Emission and Reflection Radiometer (ASTER) Global Digital Elevation Model, offer topographic information at a fine spatial scale. However, compared to the bare-earth LiDAR DEM, the global DEMs exhibit three obvious limitations. First, radar altimetry cannot penetrate water surfaces, so the global DEMs produced from radar altimetry do not provide any bathymetric information. Second, in certain regions, there may be substantial numerical discrepancies in above-water topography. The above-water DEMs demonstrate systematic overestimation caused by canopy height, and their accuracy is significantly influenced by terrain slope (Marešová et al., 2024; Simard et al., 2024). Third, the global DEMs often suffer from lower horizontal and vertical resolutions (Chen et al., 2022; Liu et al., 2019; Liu et al., 2024). Due to the limitations in global DEMs, delineation of wetland depressional areas using the advanced priority-flood algorithm also suffers from three problems: the bias in above-water topography (Fig. 1a and 1b), incompleteness and inaccuracy of wetland depressions identification (Fig. 1c), and the absence of bathymetric information (Fig. 1d) (Gdulová et al., 2020; Hawker et al., 2019; Li et al., 2011; Liu et al., 2024).

60

61

62

63

64

65

66

67

68

69

70

71

72

73

74

75

76

77

78

79

80

81

82

83

84

85

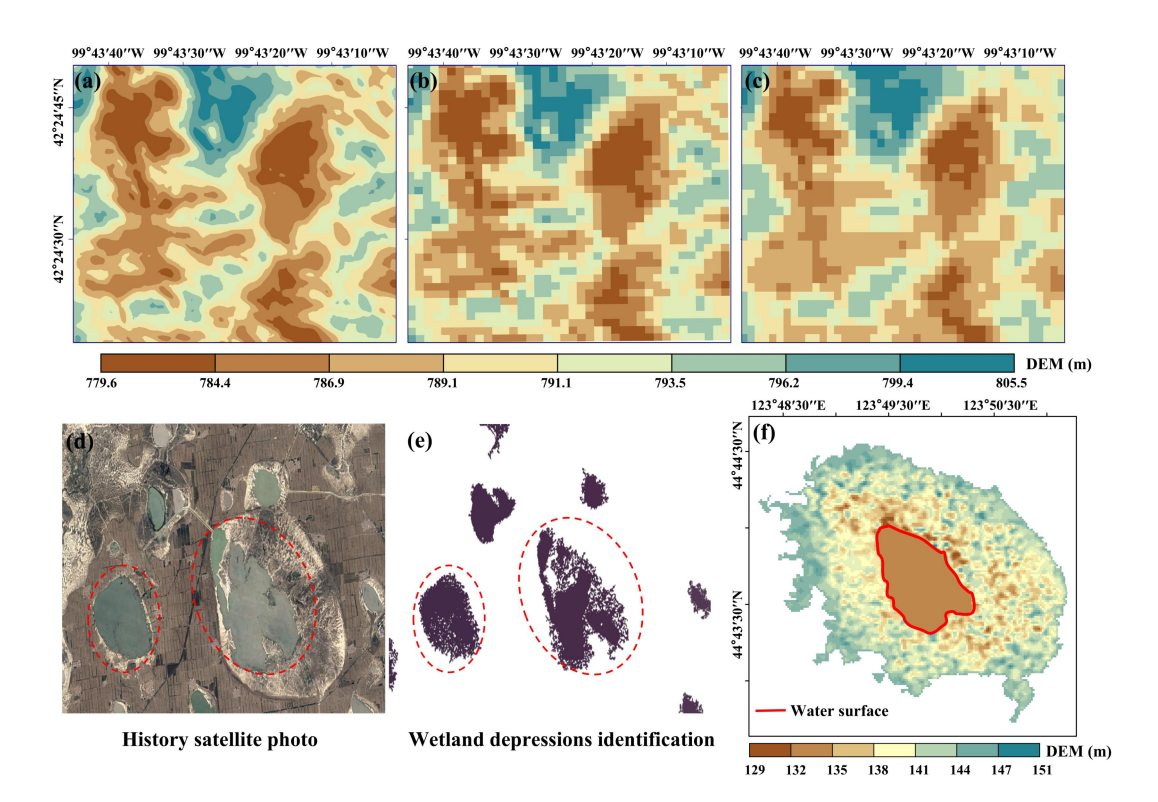


Figure 1. Wetland depression extraction based on the priority-flood algorithm and global DEMs suffers from the bias of above-water topography(Figures 1a-1c illustrate the discrepancies in above-water topography between LiDAR DEM and ALOS DEM, where Figure 1a shows the 1m spatial resolution LiDAR DEM, Figure 1b displays the LiDAR DEM resampled to 30m spatial resolution using the nearest-neighbor method, and Figure 1c presents the 30m spatial resolution ALOS DEM), incompleteness and inaccuracy of wetland depressions identification (Figure 1d shows a historical satellite image from 2013, and Figure 1e depicts the spatial distribution of wetland depressions extracted using the priority-flood algorithm and ALOS DEM, which exhibits noticeable characteristics of incomplete boundaries and spatial fragmentation), and the absence of bathymetric information (Figure 1f, where the entire water surface is represented by a single elevation value of 129 m).

In an effort to minimize the impact of the absence of bathymetric information in global DEMs on the estimation accuracy of the WDWSC, researchers have conducted studies on the estimation of underwater hypsometric relationship of wetland depressions, and the methods can be divided into two types: spatial prediction and modeling methods and remote sensing technologies. The spatial prediction and modeling methods assume that the bathymetry can be considered as a spatial extension of the surrounding exposed terrains due to long-term tectonic and geophysical evolution processes. Consequently, the underwater hypsometric relationship is assumed to be fundamentally similar to the

above-water hypsometric relationship in wetland depressions (e.g., Ahmad et al., 2020; Bonnema et al., 2016; Bonnema and Hossain, 2017; Liu and Song, 2022; Tsai et al., 2010; Vanthof and Kelly, 2019; Verones et al., 2013; Wu and Lane, 2016; Xiong et al., 2021). However, the large numerical bias in the above-water topography of global DEMs in certain regions can distort the constructed above-water hypsometric relationship of wetland depressions, thus introducing significant uncertainty to the underwater hypsometric relationship estimated by this method (Khazaei et al., 2022; Zhan et al., 2021). Over the past few decades, remote sensing technologies have demonstrated remarkable capabilities in estimating underwater hypsometric relationships at large spatial scales, facilitated by the rapid emergence of various advanced satellite sensors, including optical, passive microwave, and radar instruments (Duan and Bastiaanssen, 2013; Gao et al., 2015; Liu et al., 2022). The commonly employed approach for estimating underwater hypsometric relationship requires simultaneous observations of water area provided by optical images (e.g., Landsat series) and the corresponding water level provided by altimetry satellites (e.g., Sentinel-3, CryoSat-2, ICESat-2, Envisat). However, accuracy challenges arise due to numerical biases of altimetry satellites, cloud contamination in some optical images, and the occasional occurrence of one water area value corresponding to multiple water level values or vice versa (Li et al., 2019a; Liu et al., 2024).

In summary, previous studies using the global DEMs have overlooked critical issues such as the incompleteness and inaccuracy of wetland depression identification, as well as biases in above-water topography, leading to significant uncertainties in WDWSC estimation. In addition, insufficient attention has been paid to the drawbacks and limitations of both spatial prediction and modeling methods and remote sensing technologies in estimating bathymetry. Consequently, a comprehensive and systematic solution for the accuracy estimation of WDWSC based on the global DEMs has not yet been developed. Therefore, this study aims to develop a framework for accurately estimating WDWSC by integrating multi-source remote sensing data and prior knowledge. Specifically, we integrated priority-flood algorithm, morphological operators and prior information on water distribution map to delineate the spatial extent of wetland depressional areas. We then corrected the bias in above-water topography based on water occurrence map. Finally, we utilized remote sensing techniques to couple spatial prediction and modeling to estimate bathymetry of wetland depressional areas. The principle contribution of this developed framework, termed as WetlandSCB, lies in addressing the challenges hindering the improvement of accuracy in estimating WDWSC based on global DEMs.

#### 2 Methodology

The WetlandSCB framework can be summarized in four steps as illustrated in Figure 2. Step 1 delineation of wetland depressional areas; Step 2 above-water topography reconstruction; Step 3 bathymetric information estimation; and Step 4 hypsometric curve construction and WDWSC calculation. Each of the four steps are described in the following sections.

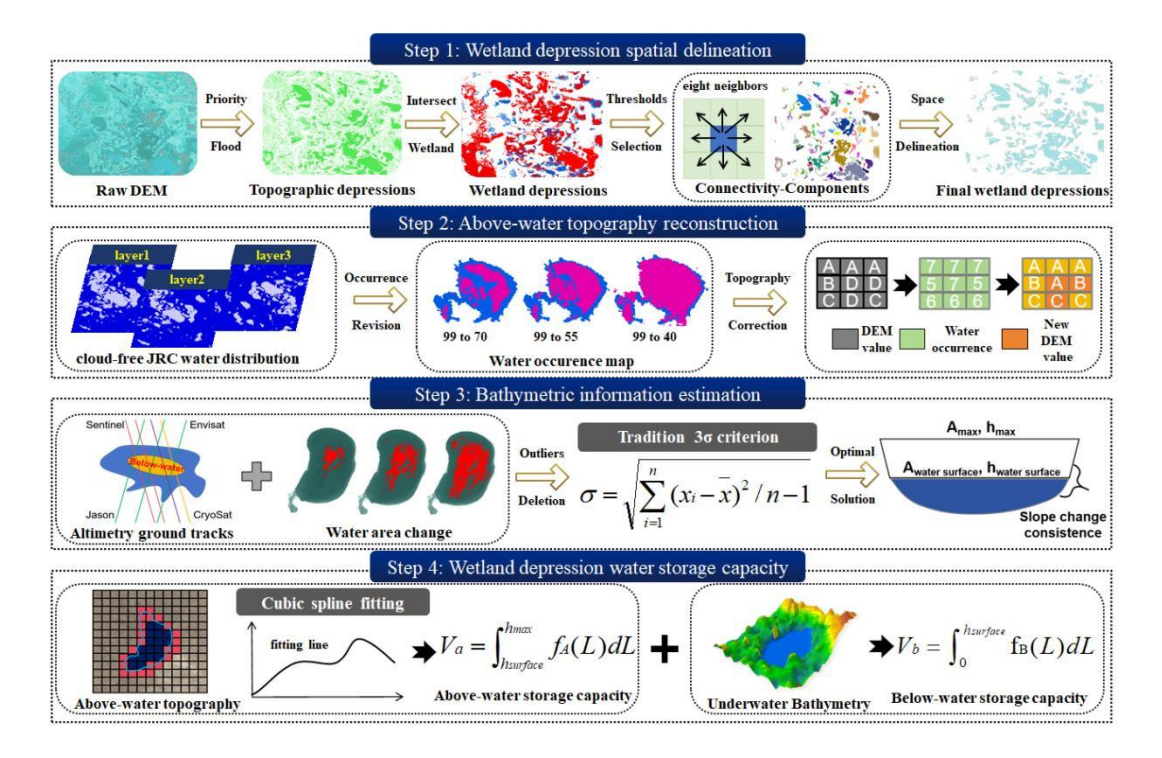


Figure 2: Flowchart of the WetlandSCB framework for accurate estimation of wetland depression water storage capacity (WDWSC) comprising four technical steps. In step 1, spatial distribution of wetland depressional areas are delineated. In step 2, wetland above-water topography is reconstruction. In step 3, bathymetric information of wetland depressional areas is estimated. In step 4, a hypsometric curve (i.e. depth-area relation) is developed and WDWSC is quantified.

#### 2.1 Wetland depression spatial delineation

We extracted the original wetland depression map from the SRTM DEM based on the priority-flood algorithm and wetland maps (Fig. 3). The priority-flood algorithm was applied to identify and fill sinks in the DEM, resulting in a depressionless DEM. By subtracting the original DEM from the depressionless DEM, an elevation difference grid was generated, where each cell value represents the depth of the depression. Subsequently, cells with elevation changes greater than zero were extracted and identified as topographic depressions. To eliminate the artifact wetland depressions, it was

necessary to transform the wetland depression map into a binary image consisting of pixels that area labeled as logical ones (wetland depression) and zeros (non-wetland depression). We then employed the eight-neighbor connectivity algorithm to extract the spatial extent of each wetland depression from the binary image. Artifact wetland depressions (e.g., rivers and channels) typically exhibit low circularity (Eq. 1) and high eccentricity (Eq. 2), whereas true wetland depressions generally display high circularity and low eccentricity. By iteratively refining the threshold values of these indicators and validating the results through visual inspection, the optimal thresholds were established to effectively eliminate artifact wetland depressions (Ahmad et al., 2020).

162 
$$Circularity = \frac{P}{2\sqrt{\pi \cdot A}}$$
 (1)

$$Eccentricity = \frac{D_f}{I_m} \tag{2}$$

where P (m) and A (m<sup>2</sup>) are the perimeter and area of the wetland depression, respectively.  $D_f$  (m) and  $L_m$  (m) represent distance between foci and the length of major axis of wetland depression.

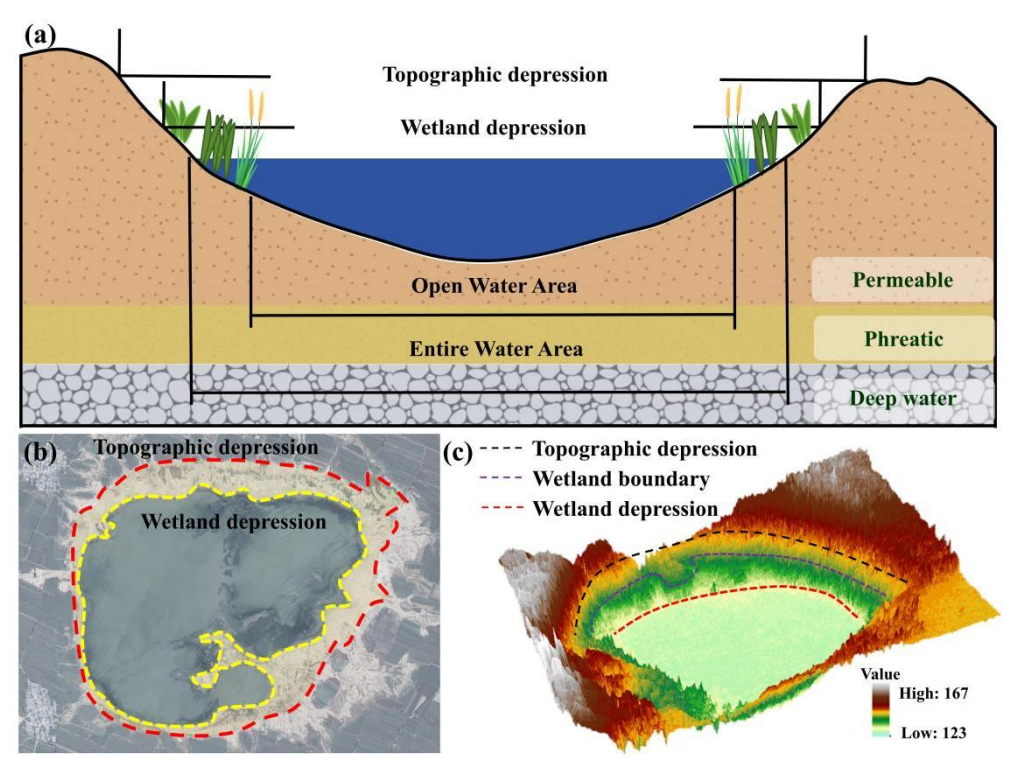


Figure 3. (a) Conceptual diagram of wetland depression profile. (b) representative wetland depressional area located in Nenjiang river basin, China. (c) 3-dimensions diagram of wetland depressional areas.

Due to incompleteness and inaccuracy identification of some wetland depressions in the original

wetland depression map (Figure 4a), morphological operators of erosion and dilation are applied for the initial spatial processes (Figure 4b). The erosion operator erodes away the boundaries of wetland depressions to enhance their edges and remove noise. The dilation operator fills up small holes (non-wetland depression pixels) surrounded by a group of wetland depression pixels (Pulvirenti et al., 2011a). The combined effect of the two operators is to remove noises while preserving the substantive features in the image. Specifically, on the Python platform, morphological opening was performed by first applying the erosion operator, followed by the dilation operator. These operations require a binary-valued kernel, where the output pixel value in the erosion step is determined by the minimum value within the kernel. A disk-shaped kernel with a 3-pixel radius was used, which is significantly smaller than typical wetland depressions but sufficient to eliminate speckle noise. The water distribution map is defined as the maximum water body distribution map, which serves as prior information, effectively characterizes the spatial extent of wetland depressions (Figure 4c). Therefore, after applying morphological operators, the wetland depression map is merged with the water distribution map within the depression boundaries through a union operation, ensuring the creation of a comprehensive and finalized wetland depression map (Figure 4d).

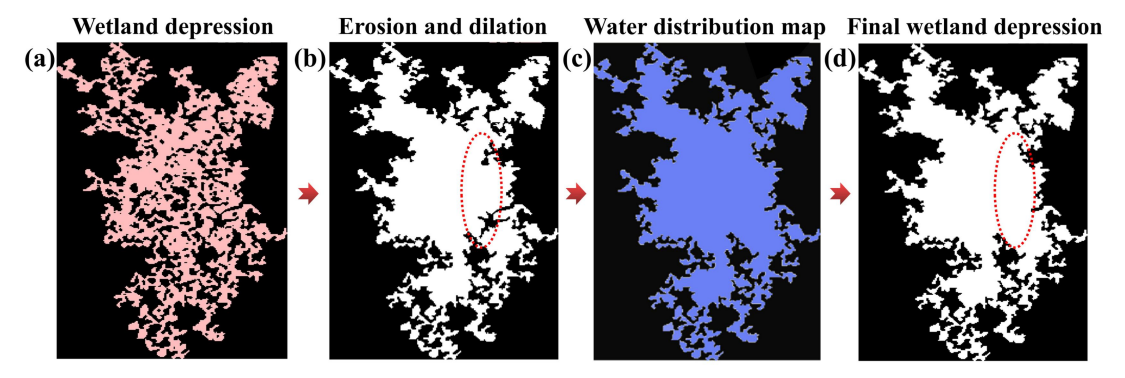


Figure 4. The final wetland depression map derived from morphological operators and prior water distribution information. Figure 4a depicts the spatial distribution of the wetland depression before processing, with pink indicating wetland depression pixels; Figure 4b shows the spatial distribution of the wetland depression after morphological operator processing, represented in white; Figure 4c illustrates the maximum water extent within the wetland depression boundaries, highlighted in blue; and Figure 4d presents the refined spatial distribution of the wetland depression, obtained by combining Figures 4b and 4c through a union operation. The red dotted polygons indicate wetland depression pixels supplemented with prior information.

#### 2.2 Above-water topography reconstruction

The basic idea is that the greater the water occurrence for a pixel (i.e., the more frequently it is covered by water), the deeper the water (Li et al., 2021). Therefore, if there is a accurate water occurrence maps, a close relationship between the water occurrence and the topography for wetland depressions can be found. The water occurrence map is generated by summing the times that the pixel is detected as water and dividing it by the number of total valid observations. The open-source Global Surface Water Mapping Layers produced by the European Commission's Joint Research Centre (JRC) contains a water occurrence map, which has been widely used to describe the topography of wetland depressions globally or in different regions (Luo et al., 2019; Pickens et al., 2020; Yao et al., 2019; Zou et al., 2018). Besides, the Global Surface Water Dynamics, produced by the Global Land Analysis & Discovery (GLAD), also includes a water occurrence map (Pickens et al., 2020). However, the cloud-free JRC water distribution images have temporal discontinuity. They are more available during dry seasons than wet seasons, which leads to deviations in the representation of real topography at the scale of individual wetland depression (Chu et al., 2020).

To address the above issue, this study proposes a method to restore the cloud-contaminated JRC water distribution images to improve the accuracy of the JRC water occurrence map. For wetland depressional areas, the JRC water distribution images are classified into cloud-free and cloud-contaminated images using the cloud screening algorithm (a rudimentary cloud-scoring algorithm called simpleCloudScore) of the Google Earth Engine platform (Mullen et al., 2021). The Canny edge detection algorithm is used to obtain the water body boundary of the two types of images (Canny, 1986). Theoretically, if the water areas are the same, the water body boundary of the cloud-free image should overlap with the exposed water body boundary in the cloud-contaminated image (Figure 5a). Therefore, by overlapping the water body boundaries of the cloud-free images with the cloud-contaminated images, the missing spatial extent of water bodies in the cloud-contaminated images can be filled. Theoretically, this method can be applicable to wetland depressional areas exceeding 0.0144 km².

The corrected JRC water occurrence map is utilized to reconstruct above-water topography. This is because the water occurrence values within the same wetland depression correspond to elevation values of SRTM DEM (Figure 5b and 5c). However, each corrected water occurrence value may correspond to multiple elevation values in the global DEMs. Therefore, the median of multiple

elevation values is used as the unique elevation value corresponding to the water occurrence value.

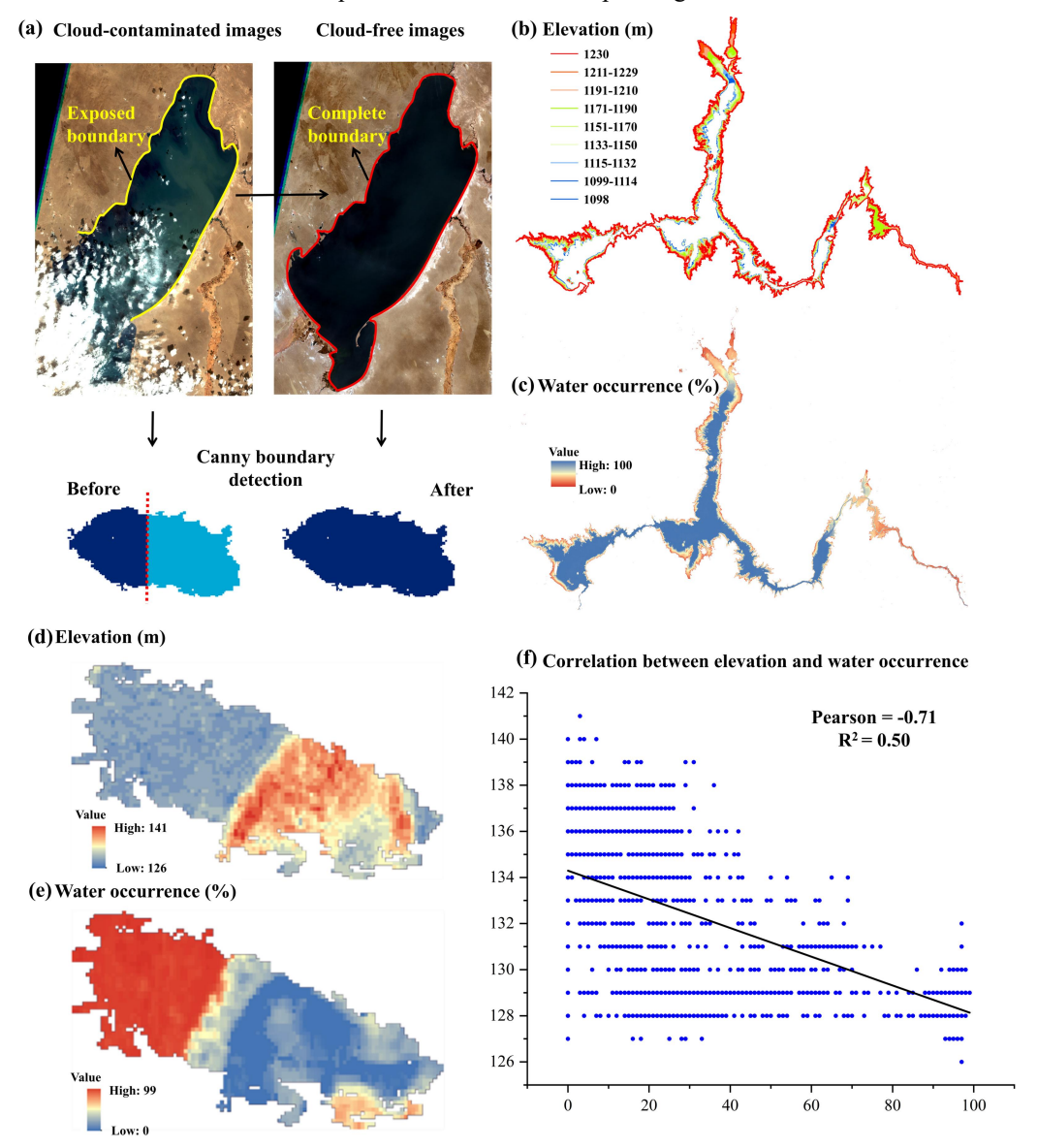


Figure 5. Above-water topography reconstruction of wetland depressional areas. (a) Restoration method of cloud-contaminated satellite images. (b) LiDAR DEM and (c) JRC water occurrence map of Mead Lakes in the United States. (d) SRTM DEM and (e) JRC water occurrence map of a representative wetland depressional area located in the Nenjiang River Basin. (f) Correlation between elevations and water occurrences in the wetland depressional area.

#### 2.3 Bathymetric information estimation

Using remote sensing technologies, simultaneous observations of water areas provided by optical images (e.g., Global Surface Water datasets) and the corresponding water levels from altimetry satellites (e.g., Sentinel-3) are employed to obtain underwater area-level pairs. Furthermore, based on

the principle of spatial prediction and modeling methods, the continuity of the slope profile between the above-water and underwater topography is used as a filtering criterion to refine the underwater area-level pairs, enabling precise characterization of the underwater topography of wetland depressions.

238

239

240

241

242

243

244

245

246

247

248

249

250

251

252

253

254

255

256

257

258

259

260

261

262

263

265

266

Match multi-source altimetry satellites with optical images to construct all area-level pairs for wetland depressions. By identifying water surface distributions in global DEMs, filter the area-level pairs that represent underwater hypsometric relationships within wetland depressions. Since altimetry satellite data are subject to various factors that influence the accuracy of water level monitoring, including intrinsic factors such as sensor performance and instrument resolution, as well as extrinsic factors like natural elements, the geometry of the wetland water body, boundary conditions, and vegetation characteristics (Zhou et al., 2023), some of the derived water level data exhibit substantial variability and uncertainty and are regarded as outliers. The outliers in the underwater area-level pairs are removed using the 3-sigma rule. Morevoer, DEM errors can be categorized into two types: systematic and random errors. To mitigate data noise, it is common practice to smooth the DEM before applying it for terrain analysis. Several filters commonly used for smoothing DEMs include median and mean filters, Gaussian filter, adaptive filter, and K-Nearest mean filter (Lindsay, 2016). In this study, we use the smoothed SRTM DEM derived from Gaussian filter to calculate the slope profile. As the slope profile is a crucial indicator reflecting the hypsometric relationship of wetland depressions (Clark and Shook, 2022; Sjöberg et al., 2022). Therefore, we first form various combinations of the processed underwater area-level pairs (each water area value uniquely corresponds to a water level value in each combination), and calculate the slope profile value  $p_u$  for each combination. Then the combination with  $p_u$  closest to the above-water slope profile  $p_a$  is taken as the optimal solution, which can effectively represent underwater bathymetry of wetland depressions.

In this study, a logarithmic transformation is applied to the calculation formula for the slope profile p of wetland depressions established by Hayashi and Van der Kamp (2000) to obtain Eq. 3. The least squares method is used to solve Eq. 3 to obtain the slope profile p value of wetland depressions:

264 
$$P = \frac{2 \cdot \ln(h_{\text{w}}/h_{\text{d}})}{\ln(A_{\text{w}}/A_{\text{d}})}$$
 (3)

where h (m), A (m<sup>2</sup>) represent the depth and area of wetland depressions, and w and d represent the different area-depth pairs.

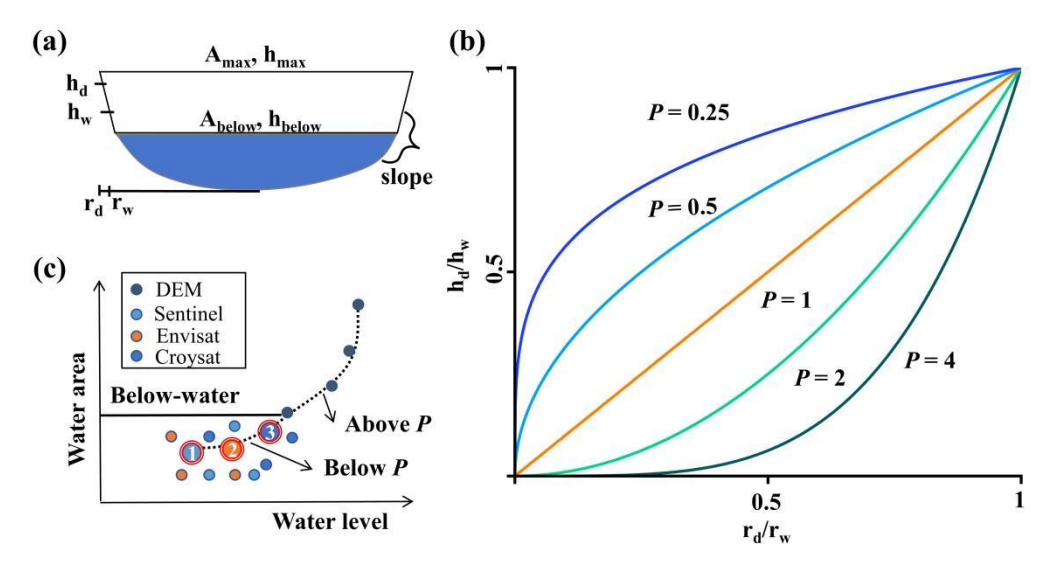


Figure 6. Estimation of bathymetric information for wetland depressional areas. (a) Schematic representation of a simplified wetland depression profile, where h (m), r (m) and A (m<sup>2</sup>) represent the depth of a wetland depressional area, the distance between the edge and the center of the wetland depression, and the area of the wetland depression, respectively. (b) Wetland depression profile for various p values. (c) Methods for bathymetric estimation of wetland depressions, where Sentinel, Envisat, and Croysat are different altimetry satellites, and the numbers 1, 2, and 3 are selected depth-area pairs.

#### 2.4 Estimation of wetland depression water storage capacity

We derived the hypsometric relationship from the corrected above-water area-level pairs and estimated underwater area-level pairs of wetland depressions. The monotonic cubic spline and power function are employed to fit the hypsometric relationships (i.e., depth-area relations) to derive the above-water hypsometric curve  $f_A(L)$  and the underwater hypsometric curve  $f_B(L)$  (Messager et al., 2016; Yao et al., 2018), respectively. Subsequently, based on the underwater hypsometric curve  $f_B(L)$ , the area enclosed by the water level from 0 to the maximum value and  $f_B(L)$  is defined as the underwater storage capacity of the wetland depression. Similarly, based on the above-water hypsometric curve  $f_A(L)$ , the area enclosed by the water level from the minimum value (corresponding to the maximum value of  $f_B(L)$ ) to the maximum value (the elevation of the spilling point) and  $f_B(L)$  is defined as the above-water storage capacity of the wetland depression. The total wetland depression water storage capacity is then obtained as the sum of both components (represented as V in Eq. 4, Figure 7).

288 
$$V = \int_{h_{watersurface}}^{h_{max}} f_A(L) dL + \int_0^{h_{watersurface}} f_B(L) dL$$
Storage Capacity

Water surface

Spline

Power

Water area

Figure 7. Schematic diagram for the estimation of wetland depression water storage capacity. Two depth-area rating curves are applied for the bathymetric volume and the above-water topographic volume.

#### 3 Validation sites and datasets

#### 3.1 Validation sites

289290

291

292

293

294

295

296

297

298

299

300

301

302

303

304

305

306

307

308

309

310

311

We applied the WetlandSCB to two wetlands in the Nenjiang River Basin (NRB), northeast China, to validate the framework. Draining a total area of 297,100 km<sup>2</sup>, the NRB is one of the largest river basins in north China. In this river basin, agricultural lands and wetlands (lakes and swamps) are prevalent (Wu et al., 2023). Recognised as critical regulators of the water balance within the NRB, wetlands are considered more important than other ecosystems in mitigating future hydrological extremes and increasing water availability for agriculture (Chen et al., 2020, Wu et al., 2020a, Wu et al., 2020b, Wu et al., 2020c). For method validation and application of the WetlandSCB framework, we focused on two national nature reserves within the NRB: the Baihe Lake and the Chagan Lake. The Baihe Lake, characterised as a marsh wetland, covers approximately 40 km<sup>2</sup>, predominantly comprising seasonal inundation zones, with an average water depth of less than 1 m. In contrast, The Chagan Lake is a large lacustrine wetland of about 372 km<sup>2</sup>, mainly composed of perennial inundation zones, with an average water depth of 2.5 m. These two validation wetlands represent different characteristics in terms of type, area, and average water depth to verify the application robustness of our developed framework. Field measurements of topographic and bathymetric information (elevation and depth) were conducted for both the Baihe Lake and the Chagan Lake, consisting of 248 and 657 measurement points, respectively (Figure 8). Specifically, we combined an ultrasonic echo sounder (D390, Chenav, China) with a Global Positioning System (GPS) positioning system and applied the

field measurements according to the sectional method. Manned vessels in areas of greater water depth and unmanned remotely operated vessels in areas of lower water depth with the aid of water rulers and hammers.

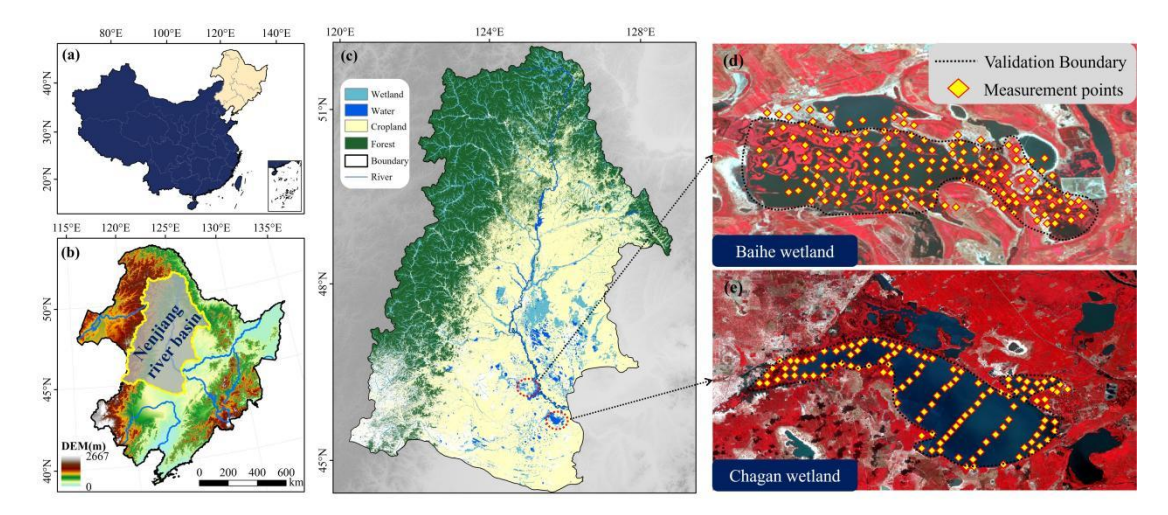


Figure 8. Locations and distribution of elevation and depth measurements across the Baihe Lake and Chagan Lake in the Nenjiang River basin, northeast China.

#### 3.2 Datasets

312

313

314

315316

317

318

319

320

321

322

323

324

325

326

327

328

329

330

331

333

The application of the WetlandSCB framework requires the following data: (i) the global DEMs sourced from SRTM DEM, with water distribution map sourced from the accompanying SRTM Water Body Data (https://earthexplorer.usgs.gov, Farr and Kobrick, 2000; NASA, 2013); (ii) wetland maps from the 30-m resolution land cover data for the years (https://zenodo.org/records/5816591, Yang and Huang, 2021) and 30-m resolution wetland map in 2015 year (http://northeast.geodata. cn/index. html, Mao et al., 2020). This study overlays the data from both sources to reduce the uncertainties in the wetland maps; (iii) water distribution maps and water occurrence map obtained from the Global Surface Water datasets (https://earthengine.google.com, Pekel et al., 2016); (iv) altimetry satellite data sourced from the Sentinel-3A/3B products (https://scihub.copernicus.eu/). In addition, pre-processing of Sentinel-3 altimetry data is performed using the geophysical and atmospheric correction method developed by Huang et al. (2019) (Eq. 5 and Eq. 6) to improve data accuracy:

$$H_{waterlevel} = H_{alt} - R - Cor$$
 (5)

where  $H_{waterlevel}$  is the water level referenced to the EGM96 geoid,  $H_{alt}$  is the altitude of the

altimeter derived from the modeling of satellite trajectory, *R* is the range computed through the time duration of the echoes, and *Cor* is referred to as the geophysical and environmental corrections:

$$Cor = C_{dry} + C_{wet} + C_{iono} + C_{solidEarth} + C_{pole} + C_{EGM96}$$

$$\tag{6}$$

where  $C_{dry}$ ,  $C_{wet}$ ,  $C_{iono}$ ,  $C_{solidEarth}$ ,  $C_{pole}$  and  $C_{EGM96}$  are the dry tropospheric, wet tropospheric, ionospheric corrections, the solid Earth tide, polar tide corrections and the EGM96 geoid respectively.

#### 4 Results and discussions

339

340

341

342

343

344

345

346

347

348

349

350

351

352

353

354

355

356

357

358

359

360

361

362

#### 4.1 Performance evaluation of wetland depression spatial delineation and uncertainty analysis

The actual topographic and bathymetric information obtained from field measurements, along with the contour-tree method, provides the actual spatial distribution of wetland depressional areas. Additionally, two spatial distributions of wetland depressional areas are derived: one using the SRTM DEM combined with the priority-flood algorithm and the other using the SRTM DEM with the WetlandSCB framework. A comparative analysis of these three approaches is conducted to assess the accuracy differences in wetland depression spatial delineation by using four indicators: overall accuracy, kappa coefficient, producer's accuracy, and user's accuracy (Fig. 9a-f). The confusion matrix, also known as an error matrix, is a crucial method for evaluating land cover classification accuracy. It intuitively reflects the classification relationship between the evaluated data and the reference data. Key evaluation metrics include the above four indicators. For detailed calculation equations, refer to Liu et al. (2007). The results indicate that the WetlandSCB framework can accurately determine the spatial distribution of wetland depressions, with all four indicators exceeding 0.95. In contrast, the user's accuracy is above 0.93 in both validation wetlands (error of commission is 0.07), and the producer's accuracy is only 0.37 (error of omission is 0.63) in Baihe Lake based on the priority-flood algorithm. Since the overall accuracy of wetland depression spatial delineation derived using the priority-flood algorithm exceeds 0.6 for both validation wetland sites, with a peak accuracy of 0.97 for Chagan Lake, the results demonstrate that the algorithm is highly effective in identifying wetland depressions, but is limited by the numerical errors of the global DEMs, which leads to lower extraction accuracy of the spatial distribution of wetland depressions (Zhou et al., 2016). Since the overall accuracy, Kappa coefficient, and Producer's accuracy of wetland depression spatial delineation obtained using the WetlandSCB framework show significant improvements over those derived from the priority-flood algorithm for both validation wetlands, with a slight increase in User's accuracy for Chagan Lake, the results effectively demonstrate that the WetlandSCB framework outperforms the priority-flood algorithm in wetland depression spatial delineation..

363

364

365

366

367

368

369

370

371

372

373

374

375

376

377

378

379

380

Uncertainty in wetland depression spatial delineation using the WetlandSCB framework primarily mainly arises from morphological operators and prior information on water distribution map. Figures 9g and 9h show that, compared with morphological operators, prior information on water distribution map can significantly alter the performance of wetland depression spatial delineation and is a key factor in determining the level of uncertainty. For instance, in Baihe Lake, the overall accuracy and kappa coefficient improved by 0.29 and 0.56, respectively, after processing with prior information on water distribution map. Similar studies have also found that the type and reliability of prior information are major factors affecting the spatial filling performance of surface water maps (Aires, 2020; Pulvirenti et al., 2011b). Therefore, this study compared the wetland depression spatial delineation results based on three sets of prior information on water distribution map: GLC-FCS30 (from Zhang et al., 2021), CLCD (from Yang and Huang, 2021), and JRC (Fig. 9i and 9j), where GLC-FCS30 and CLCD are 30-meter resolution land cover datasets, and JRC provides 30-meter resolution water surface data.. The overall accuracy differences for the Baihe Lake and Chagan Lake ranged from 0.68 to 0.98 and from 0.93 to 0.99, respectively. In general, the accuracy levels of prior information from high to low were JRC > GLC-FCS30 > CLCD. This suggests that selecting highly reliable prior information on water distribution map is an essential way to reduce uncertainty in the WetlandSCB framework.

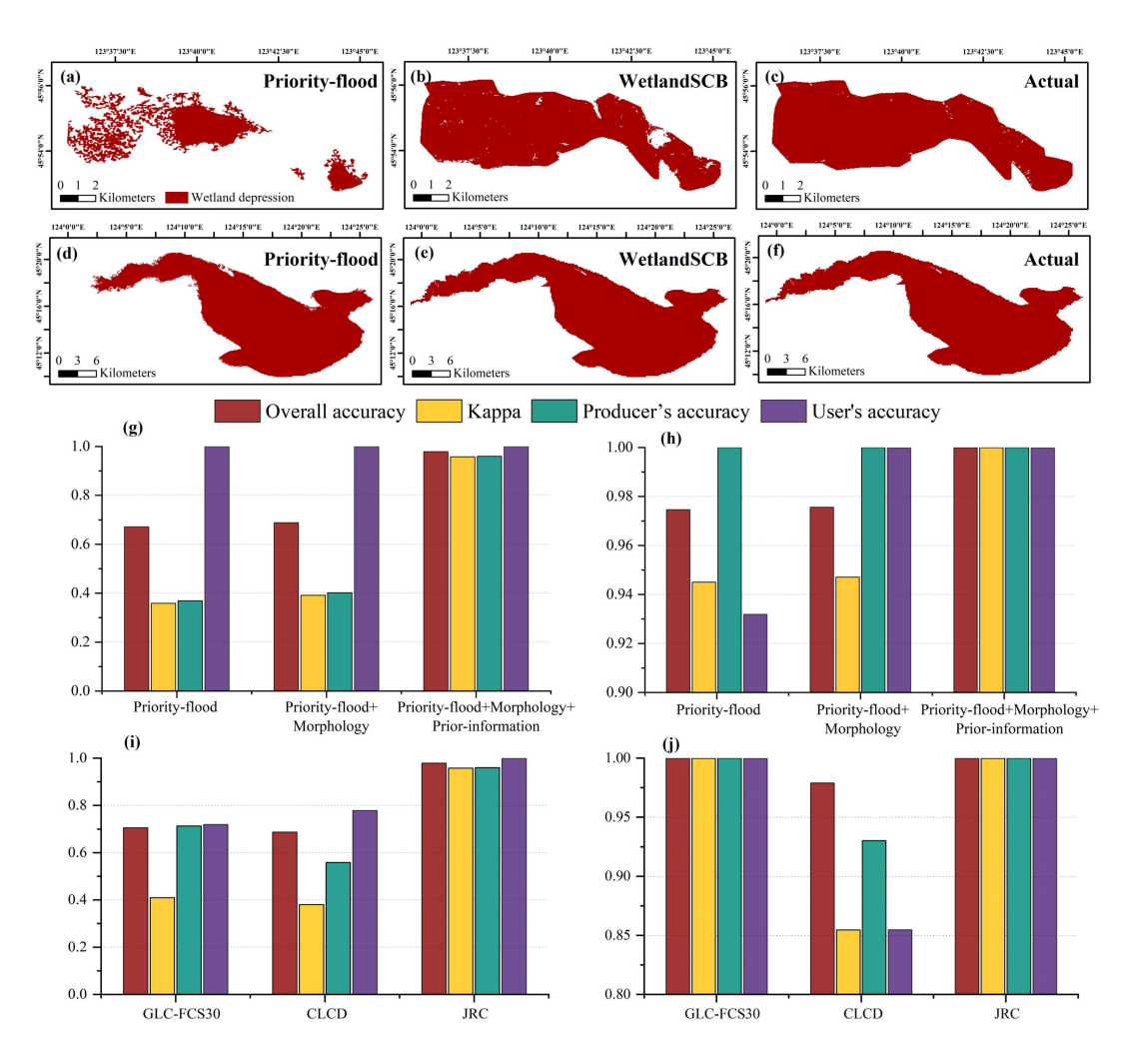


Figure 9. (a), (b), and (c) depict the spatial distribution of wetland depressional areas in the Baihe Lake based on the priority-flood algorithm, WetlandSCB framework, and field measurements (the actual wetland depression map was derived from field measurements using the contour-tree method), respectively. (d), (e), and (f) show the corresponding results for the Chagan Lake. The impact of morphological operators and prior information on water distribution map from the WetlandSCB framework is illustrated in (g) and (h). The influence of different prior information on water distribution map from the WetlandSCB framework is presented in (i) and (j).

### 4.2 Performance evaluation of above-water topography correction and uncertainty analysis

The consistency between the original and corrected above-water topography and the actual above-water topography obtained from field measurements can be evaluated using Pearson correlation coefficients and  $R^2$ . The results indicate that the consistency between the original (the elevation information directly obtained from the SRTM DEM as the original above-water topography) and actual

above-water topography is remarkably low, with R<sup>2</sup> values less than 0.2 for both validation wetlands. Previous studies have also observed significant numerical discrepancies between the original and actual above-water topography in some regions (e.g., Mukul et al., 2017; Uuemaa et al., 2020). Compared to the original results, the consistency between the corrected and actual above-water topography significantly improves. For example, the Pearson correlation coefficient and R<sup>2</sup> reach 0.74 and 0.55 in the Baihe Lake, respectively, demonstrating that the WetlandSCB framework can effectively correct numerical biases in above-water topography.

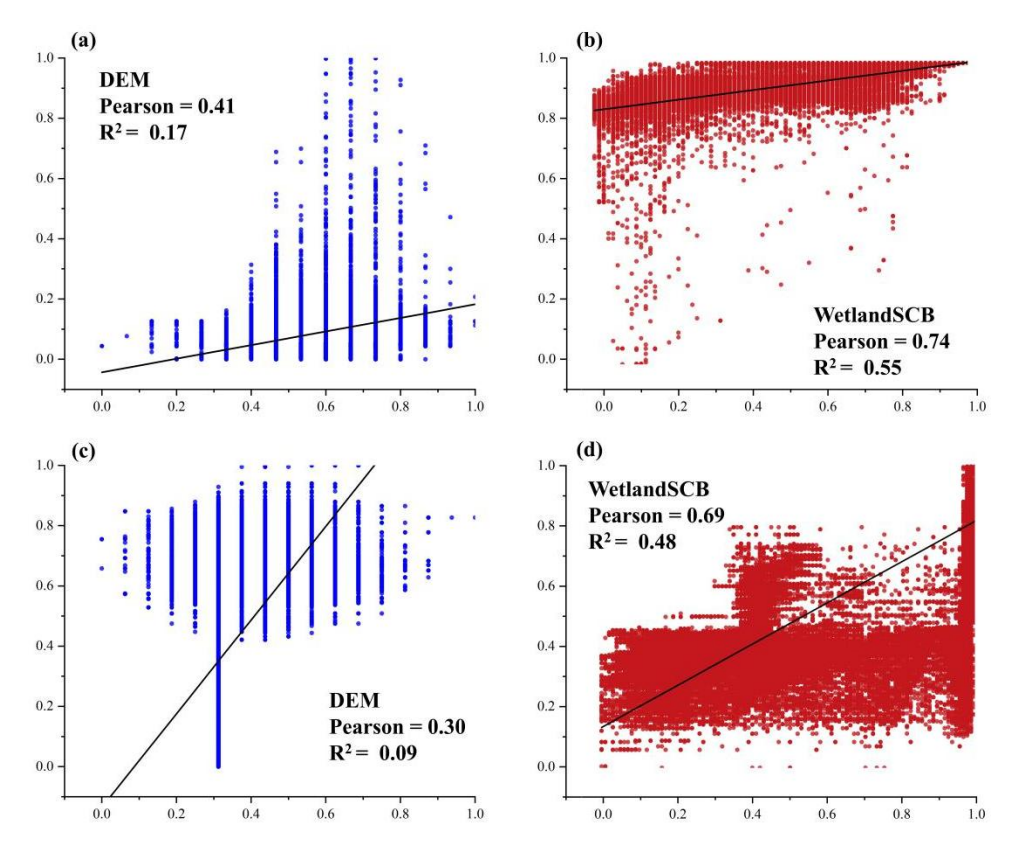


Figure 10. (a) and (b) Consistency analysis results between the original and corrected above-water topography for Baihe Lake. (c) and (d) are corresponding results for Chagan Lake. The elevation values are mapped to [0, 1] based on extreme value normalization.

Uncertainty in correcting above-water topography using the WetlandSCB framework depends primarily on the accuracy of the water occurrence map. Therefore, due to the negative relationship between water occurrence values and elevations in wetland depressions, this study compared the correlation differences between two sets of global-scale water occurrence maps, namely GLAD and JRC, and the actual above-water topography of two wetland depressions. The results show that the

correlation level of GLAD is superior to JRC in the Baihe Lake, while the opposite is observed in the Chagan Lake. Additionally, the R<sup>2</sup> values for both sets of water occurrence maps are less than 0.4 (Figure 11c-f), which is significantly lower than the accuracy level of the corrected above-water topography. This clearly shows the superiority of the water occurrence map generated by the WetlandSCB framework over the GLAD or original JRC map.

It is to note that the water occurrence map generated by the WetlandSCB framework still has a certain level of uncertainty. First, the extraction of a complete and accurate water spatial distribution from cloud-free images is constrained by factors such as the classification algorithm (Figure 11a) (Peket et al., 2016), but some correction algorithms have been proposed to enhance raw water distribution images (Zhao and Gao, 2018). Second, there is currently a lack of high-precision, temporally and spatially continuous water distribution maps (Figure 11b). Future efforts could include the use of image fusion methods, such as the Spatial and Temporal Adaptive Reflectance Fusion Mode, to fuse data from multi-source remote sensing products such as Sentinel-2, MODIS, and Landsat, which can effectively enhance the accuracy of water occurrence map (He et al., 2020; Wang et al., 2016).

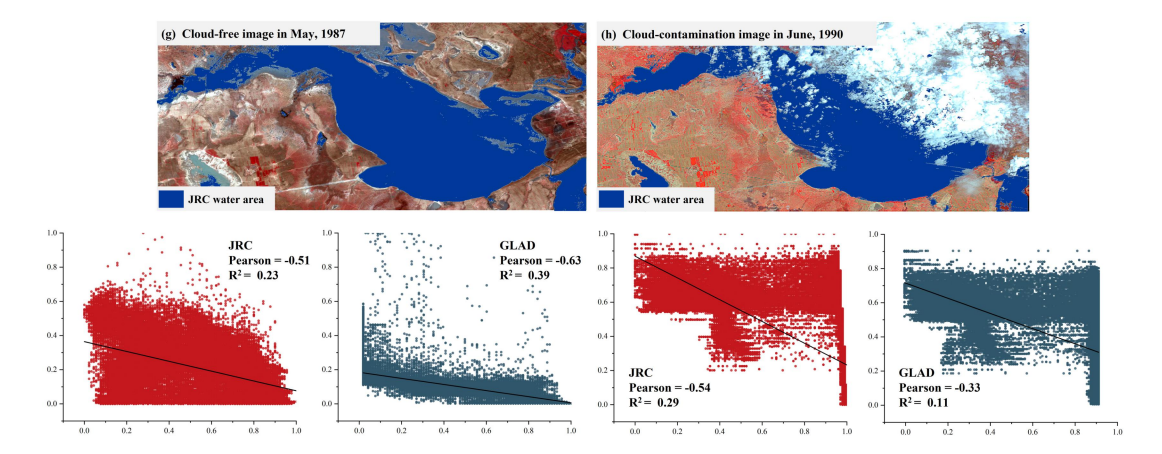


Figure 11. (a) and (b) depict sources of uncertainty in water occurrence map generated by the WetlandSCB framework. (c), (d), (e) and (f) illustrate the difference between two water occurrence maps on the performance of above-water topography correction in the Baihe Lake and the Chagan Lake.

#### 4.3 Performance evaluation of bathymetric information estimation

The slope profile p is used to describe the bathymetry of wetland depressional areas. The calculated p values for the Baihe lake and the Chagan Lake using the WetlandSCB framework are 7.45

and 4.08, respectively. The actual bathymetric information obtained from field measurements is used to construct area-depth pairs. Subsequently, the actual slope profile p of the wetland depression is calculated based on the calculation formula established by Hayashi and Van der Kamp (2000). The relative errors with respect to the actual p values obtained from field measurements are both less than 3%, demonstrating the high accuracy of the framework in estimating underwater bathymetry.

435

436

437

438

439

440

441

442

443

444

445

446

447

448

449

450

451

452

453

454

455

456

457

458

459

460

461

462

463

To further prove the superiority of the WetlandSCB framework in estimating bathymetry, this study employed spatial prediction and modeling methods, which assumes that the underwater slope profile is fundamentally similar to the above-water slope profile in wetland depressions, resulting in a p value of 8.65 for the Baihe Lake and 4.78 for the Chagan Lake. The relative errors with respect to the actual p values are both greater than 18%, indicating that this method may lead to substantial errors in some regions, as also reported by Papa et al. (2013) and Vanthof and Kelly. (2019). Furthermore, previous studies have often applied smoothing methods to the global DEMs to enhance the accuracy of topographic characterization in wetland depressions (e.g., Jones et al., 2018; Wu et al., 2019). In this regard, we further used the Gaussian-smoothed global DEMs and the spatial prediction and modelling methods to calculate p for the Baihe Lake and the Chagan Lake. The resulting values were 8.51 and 4.37, with relative errors of 17.63% and 7.9%, respectively. This underscores that smoothing methods do indeed contribute to improving the accuracy of topographic information in wetland depressions. Notably, the relative error for the Chagan Lake is significantly lower than that for the Baihe Lake, which is consistent with the findings of Liu and Song (2022), who reported that the spatial prediction and modeling methods are suitable for wetlands with long and narrow shape. In summary, the comparative analysis reveals that the WetlandSCB framework demonstrates superior performance in bathymetric estimation for wetland depressional areas. For Baihe Lake, the slope profile p derived from the WetlandSCB framework (7.45) exhibits closer agreement with the actual measured value (7.29) than those obtained from the spatial prediction and modeling method (8.65) and its enhanced version incorporating smoothed SRTM DEM (8.51). Similarly, for Chagan Lake, the WetlandSCB framework yields a slope profile p (4.08) that more accurately approximates the actual value (4.05) compared to both the conventional spatial prediction and modeling method (4.78) and its enhanced version (4.37). These comparative results demonstrate the improved accuracy and reliability of the WetlandSCB framework in bathymetric characterization of wetland depressional areas relative to the other methods.

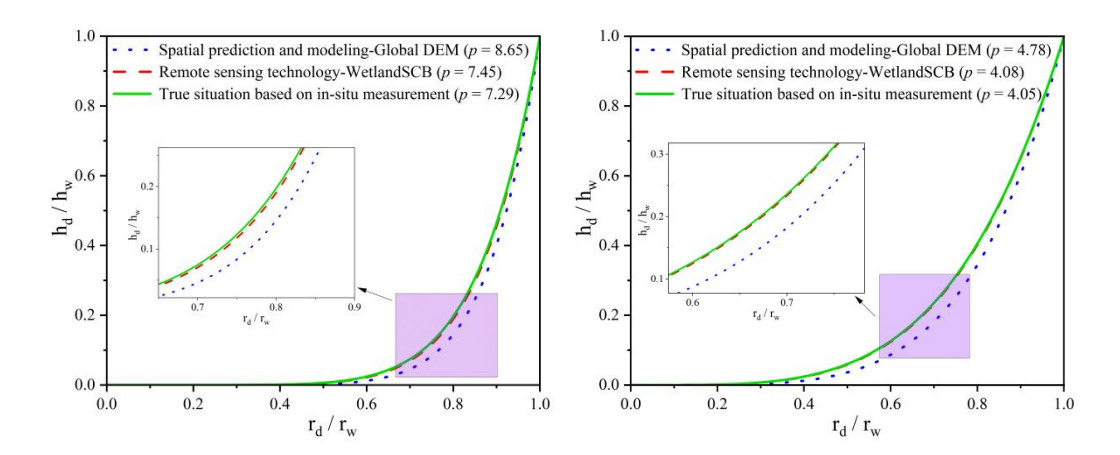


Figure 12. Slope profile p values of wetland depressions for the Baihe Lake (left) and the Chagan Lake (right), calculated with spatial prediction and modeling methods, and the WetlandSCB framework in comparison with filed measurements.

464

465

466

467

468

469

470

471

472

473

474

475

476

477

478

479

480

481

482

483

484

485

486

# 4.4 WetlandSCB framework application and implications for integrated water resources management

Wetland depressions are largely disregarded in many hydrologic modeling practices. Rare studies exist on how their exclusion can lead to potentially inaccurate model projections and understanding of hydrologic dynamics across the world's river basins (Rajib et al., 2020). This study applied a novel framework delineating the topography and bathymetry of wetland depressional areas and focusing on two distinctive wetlands to estimate WDWSC. Using the field measurements of topography and bathymetry of the Baihe Lake and the Chagan Lake, the depth-area hypsometric curves were constructed, and the WDWSC of the Baihe Lake and the Chagan Lake were estimated to be 61 million m³ and 526 million m³, respectively (Fig. 13). The estimation results based on the WetlandSCB framework were correspondingly 55 million m<sup>3</sup> and 521 million m<sup>3</sup>. Furthermore, The use of elevation (to compute wetland depression depths) and areal extent has emerged as an efficient method to estimate surface-water storage volume (Gao, 2015). After identifying wetland depressions, previous studies estimated the area and volume of each depression based on a statistical analysis of the DEM cells comprising that wetland depression (Rajib et al., 2018; Wu et al., 2019; Wu and Lane, 2016). This study compared and analyzed the water storage capacity of Baihe Lake and Chagan Lake, calculated using three medium-resolution 30-m DEM datasets: SRTM DEM, ALOS DEM, and MERIT DEM (Figure 13c). The results show that the accuracy of WDWSC calculation is highly dependent on the

DEM data quality, with the MERIT DEM providing the most accurate results, with relative errors averaging 25.7% compared to the actual WDWSC. In contrast, the WDWSC calculation based on the WetlandSCB framework had relative errors of less than 10%, which is a good level of accuracy in estimation precision (Moriasi et al., 2015), demonstrating that the WetlandSCB framework has the ability to accurately estimate WDWSC, which can be applied to regions lacking field measurement data for global-scale wetland water storage capacity estimation.

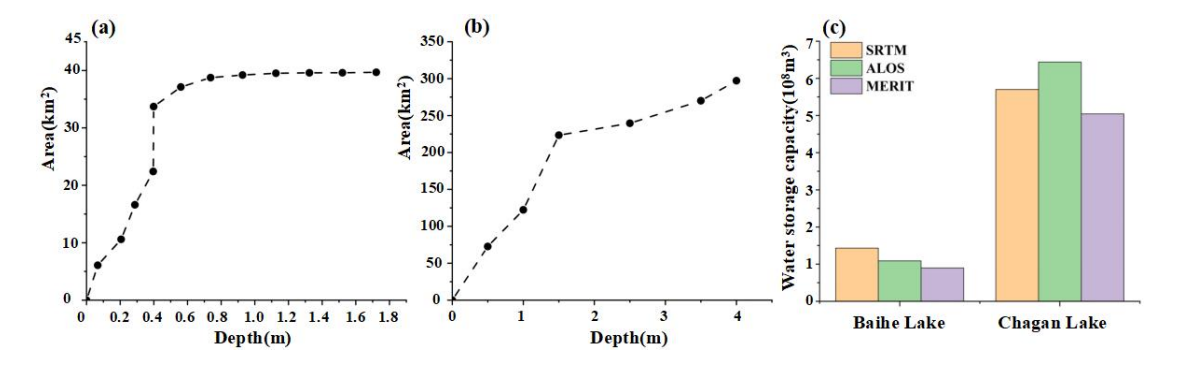


Figure 13. The dashed line represent the actual hypsometric curve based on field measurements for the Baihe Lake (a) and the Chagan Lake (b), respectively. The calculation results of WDWSC based on three DEM datasets in validation wetland sites (c).

Wetlands play a pivotal role in mitigating flood and drought risks, as well as addressing water scarcity challenge within a river basin. Previous studies underscore the significant impact of wetlands in attenuating future flood characteristics, including peak flows, mean flows, duration, and flow volume for various return period floods (Wu et al., 2023). Concurrently, wetlands contribute to enhancing baseflow during both summer and winter seasons in the NRB (Wu et al., 2020c). Given the NRB is a agriculture-dominated river basin, wetlands serves as the main water supply nodes by collecting the flash flood and storing and purifying irrigation return flows. This reclaimed water can be efficiently reused for irrigation purposes in the NRB (Meng et al., 2019; Smiley and Allred, 2011; Zou et al., 2018). The WDWSC is a key parameter for evaluating the flood control and water supply capacity of wetlands, also as a important prerequisite for understanding the impact of wetlands on extreme hydrological events (Acreman and Holden, 2013). Therefore, the developed WetlandSCB framework, which can provide accurate estimation of the WDWSC, contributes to the management of food and water security in the NRB. Against the backdrop of global environmental change, characterized by an escalation in the intensity and frequency of extreme hydrological events, and the

increasing disparity between water resource supply and demand, there is an urgent need for a novel integrated water resources management approach based on natural solutions (Rodell and Li, 2023; Thorslund et al., 2017; Yin et al., 2018). Wetlands have emerged as a nature-based solution in various water resources management practices (Ferreira et al., 2023). Taking advantage of the wetland hydrological regulation functions is instrumental in addressing the risks of flood and drought disasters arising from global climate change, land use change, as well as the water scarcity risks stemming from agricultural-ecological water competition. This can help develop effective adaptation strategies and decisions for integrated water resources management.

Additionally, using the WetlandSCB framework, raster-scale wetland depression topographic information can be accurately reconstructed. Through flow direction analysis and watershed delineation methods, key parameters such as wetland inflow and outflow locations, wetland catchment boundaries, and other related characteristics can be identified (these steps can be performed using QGIS software). By integrating the hypsometric curve, water surface distribution data, and morphological characteristics of the wetland derived from the WetlandSCB framework, the initial wetland water level, the number of wetland layers, and the corresponding area-level pairs can be determined. Field surveys provide essential data on wetland soil and vegetation properties as well as inflow volumes within the study area. Finally, the hydrological model, coupled with the wetland module, can be implemented to support wetland eco-hydrological research and integrated water resources management.

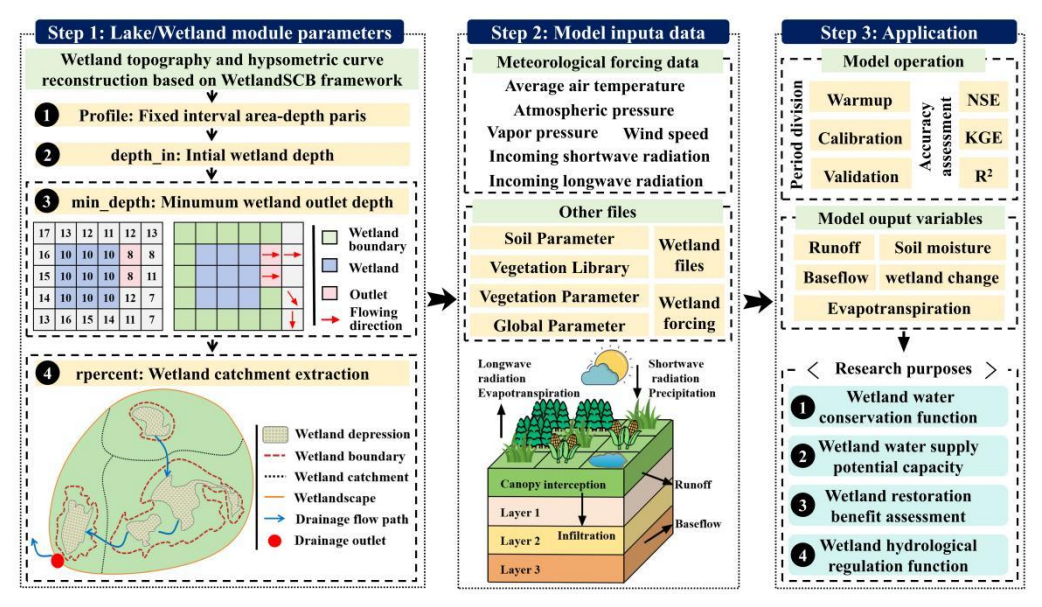


Figure 14. Integration process and application outputs of the WetlandSCB framework with VIC hydrological model.

5 Conclusions

This study developed a novel framework to accurately quantify wetland depression water storage capacity using coarse-resolution terrain data. The developed framework, WetlandSCB integrates multi-source remote sensing data, historical maps and prior knowledge, and achieved a high prediction of wetland depressional distribution and water storage capacity. This is achieved through four steps: 1) integrating priority-flood algorithm, morphological operators and prior information on water distribution maps to delineate spatial extent of wetland depressional areas; 2) correcting numerical biases in above-water topography with water occurrence map; 3) coupling spatial prediction and modeling with remote sensing techniques to estimate bathymetric information, and 4) quantifying depressional area water storage capacity based on depth-area rating curves. The conclusions are listed below:

- (1) Processing by the morphological operators and prior information on water distribution map can accurately delineate the spatial extent of wetland depressions. The derived wetland depression map shows high spatial agreement with the true wetland depression map, achieving an overall accuracy and kappa coefficient both exceeding 0.95. The performance of the WetlandSCB framework is superior to the priority-flood algorithm in wetland depression spatial delineation.
- (2) The water occurrence map can effectively correct numerical biases in above-water topography. Compared to original results, the corrected topography exhibits high consistency with true above-water topography, with average increases of 0.33 and 0.38 in Pearson coefficient and R2, respectively.
- (3) The coupling of spatial prediction and modeling methods with remote sensing techniques achieves high-precision estimation of underwater bathymetry of wetland depressions, demonstrating relative errors below 3% when compared to field measurements. The results prove that the superiority of the WetlandSCB framework over spatial prediction and modeling methods in underwater bathymetry estimation.
- (4) The WetlandSCB framework accurately estimates WDWSC with relative errors less than 10% compared to calculations based on field topography and bathymetry.

The concept and technical approaches are applicable to large-scale wetland depression water storage estimation, as well as to the regions where field measurements and/or high-resolution data are not available. Application of the WetlandSCB framework provides accurate distribution and depth-area

563 relations of wetland depressional areas which can be incorporated into wetland modules of 564 hydrological models (e.g., HYDROTEL, SWAT, HYPE, CHRM) to improve the accuracy of flow and 565 storage predictions in river basins. 566 567 Data Availability. 568 The data used in this study are openly available for research purposes. The SRTM DEM and 569 SRTM Water Body Data can be downloaded at https://earthexplorer.usgs.gov. Wetland maps are 570 available at https://zenodo.org/records/5816591 and http://northeast.geodata. cn/index. html. Water 571 distribution maps and water occurrence map are available at https://earthengine.google.com. Altimetry 572 satellite data can be downloaded at https://scihub.copernicus.eu. 573 574 Author contribution. 575 Boting Hu, Liwen chen and Yanfeng Wu designed and executed the study, all authors contributed to 576 general idea, the discussion and editing of the manuscript. 577 578 Competing interest. 579 The authors declare that they have no conflict of interest. 580 581 Acknowledgments. 582 This work was supported by the Strategic Priority Research Program of the Chinese Academy of 583 Sciences, China (XDA28020501), National Natural Science Foundation of China (41877160), National 584 Key Research and Development Program of China (2017YFC0406003, 2021YFC3200203) and The 585 Consulting Project Proposal of the Chinese Academy of Engineering (JL2023-17). 586 587 References 588 Acreman, M. and Holden, J.: How wetlands affect floods, Wetlands, 33, 773-786, https://doi.org/ 589 10.1007/s13157-013-0473-2, 2013. 590 Ahmad, S. K., Hossain, F., Pavelsky, T., Parkins, G. M., Yelton, S., Rodgers, M., Little, S., H 591 aldar, D., Ghafoor, S., Khan, R. H., Shawn, N. A., Haque, A., and Biswas, R. K.:Understan 592 ding volumetric water storage in monsoonal wetlands of Northeastern Bangladesh, Water Reso 593 ur. Res, 56(12), e2020WR027989, https://doi.org/10.1029/2020WR027989, 2020.

- 594 Aires, F., Miolane, L., Prigent, C., Pham, B., Fluet-Chouinard, E., Lehner, B., and Papa, F.: A
- 595 global dynamic long-term inundation extent dataset at high spatial resolution derived through
- downscaling of satellite observations, J. Hydrometeorol, 18(5), 1305-1325, https://doi.org/10.117
- 597 5/JHM-D-16-0155.1, 2017.
- 598 Barnes, R., Lehman, C., and Mulla, D.: Priority-flood: An optimal depression-filling and waters
- hed-labeling algorithm for digital elevation models, Comput. Geosci, 62, 117-127, https://doi.or
- 600 g/10.1016/j.cageo.2013.04.024, 2014.
- Bonnema, M., Sikder, S., Miao, Y., Chen, X., Hossain, F., Ara Pervin, I., Mahbubur Rahman,
- 602 S. M., and Lee, H.: Understanding satellite-based monthly-to-seasonal reservoir outflowestimat
- ion as a function of hydrologic controls, Water Resour. Res, 52(5), 4095-4115, https://doi.org/1
- 604 0.1002/2015WR017830, 2016.
- Bonnema, M. and Hossain, F.: Inferring reservoir operating patterns across the Mekong Basin u
- sing only space observations, Water Resour. Res, 53(5), 3791-3810, https://doi.org/10.1002/201
- 607 6WR019978, 2017.
- 608 Canny, J: A computational approach to edge detection, IEEE Trans. Pattern Anal. Mach. Intell.,
- 609 (6), 679-698, https://doi.org/ 10.1109/TPAMI.1986.4767851, 1986.
- 610 Chen, T., Song, C., Zhan, P., Yao, J., Li, Y., and Zhu, J.: Remote sensing estimation of the fl
- ood storage capacity of basin-scale lakes and reservoirs at high spatial and temporal resoluti
- ons, Sci. Total Environ, 807, 150772, https://doi.org/10.1016/j.scitotenv.2021.150772, 2022.
- 613 Chen, W., Nover, D., Yen, H., Xia, Y., He, B., Sun, W., and Viers, J.: Exploring the multiscal
- e hydrologic regulation of multipond systems in a humid agricultural catchment, WaterRes, 1
- 615 84, 115987, https://doi.org/10.1016/j.watres.2020.115987, 2020.
- 616 Chu, L., Oloo, F., Sudmanns, M., Tiede, D., Hölbling, D., Blaschke, T., and Teleoaca, I.: Moni
- toring long-term shoreline dynamics and human activities in the Hangzhou Bay, China, comb
- 618 ining daytime and nighttime EO data, Big Earth Data, 4(3), 242-264, https://doi.org/10.1080/20
- 619 964471.2020.1740491, 2020.
- 620 Clark, M. P. and Shook, K. R.: The Numerical Formulation of Simple Hysteretic Models to Si
- mulate the Large-Scale Hydrological Impacts of Prairie Depressions, Water Resour. Res, 58(1
- 622 2), e2022WR032694, https://doi.org/10.1029/2022WR032694, 2020.
- 623 Cohen, M. J., Creed, I. F., Alexander, L., Basu, N. B., Calhoun, A. J., Craft, C., D'Amico, E.,
- DeKeyser, E., Fowler, L., Golden, H. E., Jawitz, J. W., Kalla, P., Kirkman, L. K., Lane, C.
- R., Lang, M., Leibowitz, S. G., Lewis, D.B., Marton, J., McLaughlin, D. L., Mushet D. M.,
- Raanan-Kiperwas, H., Rains, M. C., Smith, L., and Walls, S. C.: Do geographically isolated
- 627 wetlands influence landscape functions?, Proc. Natl. Acad. Sci. U. S.A, 113(8), 1978-1986, ht
- 628 tps://doi.org/10.1073/pnas.1512650113, 2016.
- De Klerk, A. R., De Klerk, L. P., Oberholster, P. J., Ashton, P. J., Dini, J. A., and Holness, S.
- 630 D.: A review of depressional wetlands (pans) in South Africa, including a water quality cla
- 631 ssification system, https://doi.org/10.13140/RG.2.2.28486.06723, 2016.
- Duan, Z. and Bastiaanssen, W. G. M.: Estimating water volume variations in lakes and reservo
- irs from four operational satellite altimetry databases and satellite imagery data, RemoteSens.
- Environ, 134, 403-416, https://doi.org/10.1016/j.rse.2013.03.010, 2013.
- Evenson, G. R., Golden, H. E., Lane, C. R., McLaughlin, D. L., and D'Amico, E.: Depression
- al wetlands affect watershed hydrological, biogeochemical, and ecological functions, Ecol. App
- 637 1, 28(4), 953-966, https://doi.org/10.1002/eap.1701, 2018.

- Fang, Y., Li, H., Wan, W., Zhu, S., Wang, Z., Hong, Y., and Wang, H.: Assessment of water s
- torage change in China's lakes and reservoirs over the last three decades, Remote Sens, 11(1
- 2), 1467, https://doi.org/10.3390/rs11121467, 2019.
- Farr, T. G., and Kobrick, M.: Shuttle Radar Topography Mission produces a wealth of data, E
- os Trans. AGU, 81:583-583, https://doi.org/10.1029/EO081i048p00583, 2000.
- 643 Ferreira, C. S., Kašanin-Grubin, M., Solomun, M. K., Sushkova, S., Minkina, T., Zhao, W., and
- Kalantari, Z.: Wetlands as nature-based solutions for water management in different environ
- ments, Curr. Opin. Environ. Sci. Health, 100476, https://doi.org/10.1016/j.coesh.2023.100476, 2
- 646 023.
- 647 Gao, H.: Satellite remote sensing of large lakes and reservoirs: From elevation and area tostora
- ge, Wiley Interdisciplinary Reviews: Water, 2(2), 147-157, https://doi.org/10.1002/wat2.1065, 20
- 649 15.
- 650 Gdulová, K., Marešová, J., and Moudrý, V.: Accuracy assessment of the global TanDEM-X digit
- al elevation model in a mountain environment, Remote Sens. Environ, 241, 111724, https://doi.
- 652 org/10.1016/j.rse.2020.111724, 2020.
- Haag, K. H., Lee, T. M., Herndon, D. C., County, P., and Water, T. B.: Bathymetry and veget
- ation in isolated marsh and cypress wetlands in the northern Tampa Bay area, 2000-2004, U
- S Department of the Interior, US Geological Survey, https://lccn.loc.gov/2005452253, 2005.
- Hawker, L., Neal, J., and Bates, P.: Accuracy assessment of the TanDEM-X 90 digital elevation
- model for selected floodplain sites, Remote Sens. Environ, 232, 111319, https://doi.org/10.1016
- 658 /j.rse.2019.111319, 2019.
- 659 Hayashi, M. and Van der Kamp, G.: Simple equations to represent the volume-area-depthrelati
- ons of shallow wetlands in small topographic depressions, J. Hydrol, 237(1-2), 74-85,https://do
- i.org/10.1016/S0022-1694(00)00300-0, 2000.
- 662 He, D., Zhong, Y., and Zhang, L.: Spectral-spatial-temporal MAP-based sub-pixel mappingfor l
- and-cover change detection, IEEE Trans. Geosci. Remote Sensing, 58(3), 1696-1717, https://doi.
- 664 or10.1109/TGRS.2019.2947708, 2019.
- Huang, Q., Li, X., Han, P., Long, D., Zhao, F., and Hou, A.: Validation and application of wa
- ter levels derived from Sentinel-3A for the Brahmaputra River, SCI CHINA. TECHNOL SC,
- 667 1760-1772, https://doi.org/10.1007/s11431-019-9535-3, 2019.
- Huang, S., Young, C., Feng, M., Heidemann, K., Cushing, M., Mushet, D. M., and Liu, S.:
- Demonstration of a conceptual model for using LiDAR to improve the estimation of floodwa
- ter mitigation potential of prairie pothole region wetlands, J. Hydrol, 405(3-4),417-426, https:
- 671 //doi.org/10.1016/j.jhydrol.2011.05.040, 2011.
- Jones, C. N., Evenson, G. R., McLaughlin, D. L., Vanderhoof, M. K., Lang, M. W., McCarty,
- G. W., Golden, E. H., Lane, C.R., and Alexander, L. C.: Estimating restorable wetland water
- 674 storage at landscape scales, Hydrol. Process, 32(2), 305-313, https://doi.org/10.1002/hyp.11405,
- 675 2018.
- 676 Kessler, A. C. and Gupta, S. C.: Drainage impacts on surficial water retention capacity of a pra
- irie pothole watershed, J. Am. Water Resour. Assoc, 1-13, https://doi.org/ 10.1111/jawr.12288,
- 678 2015.
- 679 Khazaei, B., Read, L. K., Casali, M., Sampson, K. M., and Yates, D. N.: GLOBathy, the glob
- al lakes bathymetry dataset, Sci. Data, 9(1), 36, https://doi.org/10.1038/ s41597-022-01132-9, 2
- 681 022.

- Lane, C. R. and D'Amico, E.: Calculating the ecosystem service of water storage in isolated
- 683 wetlands using LiDAR in North Central Florida, USA, Wetlands, 30, 967-977, https://doi.org/
- 684 10.1007/s13157-010-0085-z, 2010.
- Lane, C. R., Leibowitz, S. G., Autrey, B. C., LeDuc, S. D., and Alexander, L. C.: Hydrologica
- 686 l, physical, and chemical functions and connectivity of non-floodplain wetlands to downstrea
- 687 m waters: A review, J. Am. Water Resour. Assoc, 54(2), 346-371, https://doi.org/10.1111/1752-
- 688 1688.12633, 2018.
- 689 Lindsay, J. B.: Whitebox GAT: A case study in geomorphometric analysis, Comput. Geosci, 95,
- 75-84, https://doi.org/10.1016/j.cageo.2016.07.003, 2016.
- 691 Liu, C., Frazier, P., and Kumar, L.: Comparative assessment of the measures of thematic classi
- fication accuracy, Remote Sens. Environ, 107(4), 606-616, https://doi.org/10.1016/ j.rse.2006.10.
- 693 010, 2007.
- 694 Liu, K. and Song, C.: Modeling lake bathymetry and water storage from DEM data constraine
- d by limited underwater surveys, J. Hydrol, 604, 127260, https://doi.org/10.1016/j.jhydrol.2021.
- 696 127260, 2022.
- 697 Liu, K., Song, C., Ke, L., Jiang, L., Pan, Y., and Ma, R.: Global open-access DEM performan
- 698 ces in Earth's most rugged region High Mountain Asia: Amulti-level assessment. Geomorphol
- 699 ogy, 338, 16-26, https://doi.org/10.1016/j.geomorph.2019.04.012, 2019.
- 700 Liu, K., Song, C., Zhan, P., Luo, S., and Fan, C.: A Low-Cost Approach for Lake Volume Est
- 701 imation on the Tibetan Plateau: Coupling the Lake Hypsometric Curve and Bottom Elevatio
- 702 n, Front. Earth Sci, 10, 925944, https://doi.org/10.3389/feart.2022.925944, 2022.
- 703 Liu, K., Song, C., Zhao, S., Wang, J., Chen, T., Zhan, P., Fan, C., and Zhu, J.: Mapping inun
- dated bathymetry for estimating lake water storage changes from SRTM DEM: A global inve
- 705 stigation., Remote Sens. Environ, 301, 113960, https://doi.org/10.1016/j.rse.2023.113960, 2024.
- 706 Li, S., MacMillan, R. A., Lobb, D. A., McConkey, B. G., Moulin, A., and Fraser, W. R.: Lida
- 707 r DEM error analyses and topographic depression identification in a hummocky landscape in
- the prairie region of Canada, Geomorphology, 129(3-4), 263-275, https://doi.org/10.1016/j.geo
- 709 morph.2011.02.020, 2011.
- 710 Li, X., Ling, F., Foody, G. M., Boyd, D. S., Jiang, L., Zhang, Y., Zhou, P., Wang, Y., Chen,
- 711 R., and Du, Y.: Monitoring high spatiotemporal water dynamics by fusing MODIS, Landsat,
- water occurrence data and DEM, Remote Sens. Environ, 265, 112680, https://doi.org/10.1016/j.
- 713 rse.2021.112680, 2021.
- 714 Li, X., Long, D., Huang, Q., Han, P., Zhao, F., and Wada, Y.: High-temporal-resolution water l
- 715 evel and storage change data sets for lakes on the Tibetan Plateau during 2000-2017using m
- 716 ultiple altimetric missions and Landsat-derived lake shoreline positions, Earth Syst. Sci. Dat
- 717 a, 11(4), 1603-1627, https://doi.org/10.5194/essd-11-1603-2019, 2019a.
- 718 Li, Y., Gao, H., Jasinski, M. F., Zhang, S., and Stoll, J. D.: Deriving high-resolution reservoir
- bathymetry from ICESat-2 prototype photon-counting lidar and landsat imagery, IEEE Trans.
- 720 Geosci. Remote Sensing, 57(10), 7883-7893, https://doi.org/10.1109/TGRS.2019.2917012, 2019
- 721 b.
- 722 Luo, S., Song, C., Liu, K., Ke, L., and Ma, R.: An effective low-cost remote sensing approac
- h to reconstruct the long-term and dense time series of area and storage variations for large 1
- 724 akes, Sensors, 19(19), 4247, https://doi.org/10.3390/s19194247, 2019.

- Mao, D., Wang, Z., Du, B., Li, L., Tian, Y., Jia, M., Zeng, Y., Song, K. Jiang, M., and Wang,
- Y:: National wetland mapping in China: A new product resulting from object-based and hier
- archical classification of Landsat 8 OLI images, ISPRS-J. Photogramm. Remote Sens, 164, 11
- 728 -25, https://doi.org/10.1016/j.isprsjprs.2020.03.020, 2020.
- 729 Marešová, J., Bašta, P., Gdulová, K., Barták, V., Kozhoridze, G., Šmída, J., Markonis, Y., Rocc
- hini, D., Prošek, J., Pracná, P., and Moudrý, V.: Choosing the optimal global digital elevatio
- n model for stream network delineation: Beyond vertical accuracy, Earth Space Sci, 11(12), p.
- 732 e2024EA003743, https://doi.org/10.1029/2024EA003743, 2024.
- 733 Meng, B., Liu, J. L., Bao, K., and Sun, B.: Water fluxes of Nenjiang River Basin with ecolog
- 734 ical network analysis: Conflict and coordination between agricultural development andwetland
- 735 restoration, J. Clean Prod, 213, 933-943, https://doi.org/10.1016/j.jclepro.2018.12.243,2019.
- 736 Messager, M. L., Lehner, B., Grill, G., Nedeva, I., and Schmitt, O.: Estimating the volume an
- d age of water stored in global lakes using a geo-statistical approach, Nat. Commun, 7, 136
- 738 03, https://doi.org/10.1038/ncomms13603, 2016.
- 739 Moriasi, D. N., Gitau, M. W., Pai, N., and Daggupati, P.: Hydrologic and water quality models:
- Performance measures and evaluation criteria, Trans. ASABE, 58(6), 1763-1785, https://doi.or
- 741 g/10.13031/trans.58.10715, 2015.
- 742 Mukul, M., Srivastava, V., Jade, S., and Mukul, M.: Uncertainties in the shuttle radar topograp
- hy mission (SRTM) Heights: Insights from the indian Himalaya and Peninsula, Sci Rep, 7(1),
- 744 41672, https://doi.org/10.1038/srep41672, 2017.
- 745 Mullen, C., Penny, G., and Müller, M. F.: A simple cloud-filling approach for remote sensing
- water cover assessments, Hydrol. Earth Syst. Sci., 25, 2373-2386, https://doi.org/ 10.5194/hess
- 747 -25-2373-2021, 2021.
- 748 NASA JPL.: NASA Shuttle Radar Topography Mission Water Body Data Shapefiles & Raster
- Files [Data set]. NASA EOSDIS Land Processes Distributed Active Archive Center, Accessed
- 750 2025-02-04, https://doi.org/10.5067/MEaSUREs/SRTM/SRTMSWBD.003, 2013.
- 751 Papa, F., Frappart, F., Güntner, A., Prigent, C., Aires, F., Getirana, A. C., and Maurer, R.:Surfa
- 752 ce freshwater storage and variability in the Amazon basin from multi-satellite observations, 1
- 753 993–2007, J. Geophys. Res.-Atmos, 118(21), 11-951, https://doi.org/10.1002/2013JD020500, 201
- 754 3
- 755 Pekel, J. F., Cottam, A., Gorelick, N., and Belward, A. S.: High-resolution mapping of global
- 756 surface water and its long-term changes, Nature, 540(7633), 418-422, https://doi.org/10.1038/n
- 757 ature 20584, 2016.
- 758 Pickens, A. H., Hansen, M. C., Hancher, M., Stehman, S. V., Tyukavina, A., Potapov, P., Marr
- oquin, B., and Sherani, Z.: Mapping and sampling to characterize global inland waterdynami
- 760 cs from 1999 to 2018 with full Landsat time-series, Remote Sens. Environ, 243,111792, https:
- 761 //doi.org/10.1016/j.rse.2020.111792, 2020.
- 762 Pulvirenti, L., Chini, M., Pierdicca, N., Guerriero, L., and Ferrazzoli, P.: Flood monitoringusing
- 763 multi-temporal COSMO-SkyMed data: Image segmentation and signature interpretation, Rem
- 764 ote Sens. Environ, 115(4), 990-1002, https://doi.org/10.1016/j.rse.2010.12.002, 2011a.
- 765 Pulvirenti, L., Pierdicca, N., Chini, M., and Guerriero, L.: An algorithm for operational flood
- mapping from Synthetic Aperture Radar (SAR) data using fuzzy logic, Nat. Hazards Earth Sy
- 767 st. Sci, 11(2), 529-540, https://doi.org/10.5194/nhess-11-529-2011, 2011b.

- Rajib, A., Golden, H. E., Lane, C. R., and Wu, Q.: Surface depression and wetland waterstora
- ge improves major river basin hydrologic predictions, Water Resour. Res, 56(7), e2019WR026
- 770 561, https://doi.org/10.1029/2019WR026561, 2020.
- 771 Rodell, M. and Li, B.: Changing intensity of hydroclimatic extreme events revealed by GRAC
- 772 E and GRACE-FO, Nat. Water, 1(3), 241-248, https://doi.org/10.1038/s44221-023-00040-5, 202
- 773 3.
- 774 Shook, K., Papalexiou, S., and Pomeroy, J. W.: Quantifying the effects of Prairie depressional
- storage complexes on drainage basin connectivity, J. Hydrol, 593, 125846, https://doi.org/10.10
- 776 16/j.jhydrol.2020.125846, 2021.
- 777 Simard, M., Denbina, M., Marshak, C., and Neumann, M.: A global evaluation of radar-derived
- digital elevation models: SRTM, NASADEM, and GLO-30, J. Geophys. Res.-Biogeosci, 129
- 779 (11), e2023JG007672, https://doi.org/10.1029/2023JG007672, 2024.
- 780 Sjöberg, Y., Dessirier, B., Ghajarnia, N., Jaramillo, F., Jarsjö, J., Panahi, D. M., Xu, D., Zou,
- 781 L., and Manzoni, S.: Scaling relations reveal global and regional differences in morphometry
- of reservoirs and natural lakes, Sci. Total Environ, 822, 153510, https://doi.org/10.1016/j.scitot
- 783 env.2022.153510, 2022.
- 784 Smiley Jr, P. C. and Allred, B. J.: Differences in aquatic communities between wetlands create
- d by an agricultural water recycling system, Wetl. Ecol. Manag, 19(6), 495-505, https://doi.or
- 786 g/10.1007/s11273-011-9231-5, 2011.
- 787 Thorslund, J., Jarsjo, J., Jaramillo, F., Jawitz, J. W., Manzoni, S., Basu, N. B., Chalov, M.J., C
- reed, I. F., Goldenberg, R., Hylin, A., Kalantari, Z., Koussis, A. D., Lyon, S. W., Mazi, K.,
- Mard, J., Persson, K., Pietro, J., Prieto, C., Quin, A., and Destouni, G.: Wetlands as large-sc
- ale nature-based solutions: Status and challenges for research, engineeringand management, Ec
- 791 ol. Eng, 108, 489-497, https://doi.org/10.1016/j.ecoleng.2017.07.012, 2017.
- 792 Tsai, J. S., Venne, L. S., McMurry, S. T., and Smith, L. M.: Vegetation and land use impact o
- 793 n water loss rate in playas of the Southern High Plains, USA, Wetlands, 30, 1107-1116, https:
- 794 //doi.org/10.1007/s13157-010-0117-8, 2010.
- 795 Uuemaa, E., Ahi, S., Montibeller, B., Muru, M., and Kmoch, A.: Vertical accuracy of freely av
- ailable global digital elevation models (ASTER, AW3D30, MERIT, TanDEM-X, SRTM, and N
- 797 ASADEM), Remote Sens, 12(21), 3482, https://doi.org/10.3390/rs12213482, 2020.
- 798 Vanthof, V. and Kelly, R.: Water storage estimation in ungauged small reservoirs with the Tan
- 799 DEM-X DEM and multi-source satellite observations, Remote Sens. Environ, 235, 111437, htt
- 800 ps://doi.org/10.1016/j.rse.2019.111437, 2019.
- 801 Verones, F., Pfister, S., and Hellweg, S.: Quantifying area changes of internationally important
- wetlands due to water consumption in LCA, Environ. Sci. Technol, 47(17), 9799-9807, https://
- 803 doi.org/10.1021/es400266v, 2013.
- 804 Wang, Q., Shi, W., and Atkinson, P. M.: Spatiotemporal subpixel mapping of time-series image
- 805 s, IEEE Trans. Geosci. Remote Sensing, 54(9), 5397-5411, https://doi.org/10.1109/TGRS.2016.
- 806 2562178, 2016.
- 807 Wu, Q., Lane, C. R., Wang, L., Vanderhoof, M. K., Christensen, J. R., and Liu, H.: Efficient
- 808 delineation of nested depression hierarchy in digital elevation models for hydrological analysi
- s using level-set method, J. Am. Water Resour. Assoc, 55(2), 354-368, https://doi.org/10.1111/1
- 810 752-1688.12689, 2019.

- 811 Wu, Q. and Lane, C. R.: Delineation and quantification of wetland depressions in the Prairie P
- othole Region of North Dakota, Wetlands, 36(2), 215-227, https://doi.org/10.1007/s13157-015-0
- 813 731-6, 2016.
- 814 Wu, Y., Sun, J., Blanchette, M., Rousseau, A. N., Xu, Y. J., Hu, B., and Zhang, G.: Wetland
- 815 mitigation functions on hydrological droughts: From drought characteristics to propagation of
- meteorological droughts to hydrological droughts, J. Hydrol, 617, 128971, https://doi.org/10.10
- 817 16/J.JHYDROL.2022.128971, 2023.
- 818 Wu, Y., Sun, J., Xu, Y. J., Zhang, G., and Liu, T.: Projection of future hydrometeorological ex
- 819 tremes and wetland flood mitigation services with different global warming levels: A case st
- udy in the Nenjiang river basin, Ecol. Indic, 140, 108987, https://doi.org/10.1016/j.ecolind.2022.
- 821 108987, 2022a.
- 822 Wu, Y., Zhang, G., Rousseau, A. N., and Xu, Y. J.: Quantifying streamflow regulation services
- of wetlands with an emphasis on quickflow and baseflow responses in the Upper Nenjiang
- 824 River Basin, Northeast China, J. Hydrol, 583, 124565, https://doi.org/10.1016/j.jhydrol.2020.124
- 825 565, 2020b.
- 826 Wu, Y., Zhang, G., Rousseau, A. N., Xu, Y. J., and Foulon, É.: On how wetlands can provide
- flood resilience in a large river basin: a case study in Nenjiang river Basin, China, J.Hydro
- 828 l, 587, 125012, https://doi.org/10.1016/j.jhydrol.2020.125012, 2020c.
- 829 Xiong, L., Tang, G., Yang, X., and Li, F.: Geomorphology-oriented digital terrain analysis:Progr
- ess and perspectives, J. Geogr. Sci, 31, 456-476, https://doi.org/10.1007/s11442-021-1853-9, 2
- 831 021.
- Yang, J. and Huang, X.: 30 m annual land cover and its dynamics in China from 1990 to 20
- 833 19, Earth Syst. Sci. Data, 2021, 1-29. https://doi.org/10.5194/essd-13-3907-2021, 2021.
- Yao, F., Wang, J., Wang, C., and Crétaux, J. F.: Constructing long-term high-frequency time se
- 835 ries of global lake and reservoir areas using Landsat imagery, Remote Sens. Environ, 232, 11
- 836 1210, https://doi.org/10.1016/j.rse.2019.111210, 2019.
- 837 Yao, F., Wang, J., Yang, K., Wang, C., Walter, B. A., and Crétaux, J. F.: Lake storage variatio
- n on the endorheic Tibetan Plateau and its attribution to climate change since the newmillen
- 839 nium, Environ. Res. Lett, 13(6), 064011, https://doi.org/10.1088/1748-9326/aab5d3,2018.
- Yin, J., Gentine, P., Zhou, S., Sullivan, S. C., Wang, R., Zhang, Y., and Guo, S.: Large increa
- se in global storm runoff extremes driven by climate and anthropogenic changes, Nat.Commu
- n, 9(1), 4389, https://doi.org/10.1038/s41467-018-06765-2, 2018.
- 843 Zhan, P., Song, C., Luo, S., Liu, K., Ke, L., and Chen, T.: Lake level reconstructed from DE
- 844 M-based virtual station: Comparison of multisource DEMs with laser altimetryand UAV-LiDA
- R measurements, IEEE Trans. Geosci. Remote. Sens, 19, 1-5, https://doi.org/ 10.1109/LGRS.2
- 846 021.3086582, 2021.
- 847 Zhang, X., Liu, L., Chen, X., Gao, Y., Xie, S., and Mi, J.: GLC FCS30: Global land-cover pr
- 848 oduct with fine classification system at 30 m using time-series Landsat imagery, EarthSyst. S
- ci. Data, 13(6), 2753-2776, https://doi.org/10.5194/essd-13-2753-2021, 2021.
- 850 Zhao, G. and Gao, H.: Automatic correction of contaminated images for assessment of reservoi
- 851 r surface area dynamics, Geophys. Res. Lett, 45(12), 6092-6099, https://doi.org/10.1029/2018G
- 852 L078343, 2018.

- 853 Zhou, G., Sun, Z., and Fu, S.: An efficient variant of the priority-flood algorithm for filling d
- epressions in raster digital elevation models, Comput. Geosci, 90, 87-96, https://doi.org/10.1016
- 855 /j.cageo.2016.02.021, 2016.
- 856 Zhou, H., Liu, S., Mo, X., Hu, S., Zhang, L., Ma, J., Bandini, F., Grosen, H., and BauerGott
- 857 wein, P.: Calibrating a hydrodynamic model using water surface elevation determined from I
- 858 CESat-2 derived cross-section and Sentinel-2 retrieved sub-pixel river width. Remote Sens. E
- nviron. 298, 113796. https://doi.org/10.1016/j. rse.2023.113796, 2023.
- 860 Zou, Y., Wang, L., Xue, Z., E, M., Jiang, M., Lu, X., Yang, S., Shen, X., Liu, Z., Sun, G., a
- 861 nd Yu, X.: Impacts of agricultural and reclamation practices on wetlands in the AmurRiver
- 862 Basin, Northeastern China, Wetlands, 38, 383-389, https://doi.org/10.1007/s13157-017-0975-4, 2
- 863 018.
- Zou, Z., Xiao, X., Dong, J., Qin, Y., Doughty, R. B., Menarguez, M. A., Zhang, C., and Wan
- g, J.: Divergent trends of open-surface water body area in the contiguous United States from
- 866 1984 to 2016, Proc. Natl. Acad. Sci. U. S. A, 115(15), 3810-3815, https://doi.org/10.1073/pna
- 867 s.1719275115, 2018.